Lithos 324–325 (2019) 454–465

Contents lists available at ScienceDirect

Lithos

journal homepage: www.elsevier.com/locate/lithos

Zinc isotopic compositions of migmatites and granitoids from the Dabie Orogen, central China: Implications for zinc isotopic fractionation during differentiation of the continental crust

Li-Juan Xu *, Sheng-Ao Liu *, Ze-Zhou Wang, Chunyang Liu, Shuguang Li

State Key Laboratory of Geological Processes and Mineral Resources, China University of Geosciences, Beijing 100083, China

ARTICLE INFO

Article history:
Received 11 August 2018
Accepted 22 November 2018
Available online 26 November 2018

Keywords:
Zinc isotopes
Isotope fractionation
Granitic differentiation
Migmatite
Dabie orogen

ABSTRACT

Some high silica granitic rocks (SiO_2 > 70 wt%) show larger Zn isotopic variations ($\delta^{66}Zn_{JMC\ 3\text{-}0749L}$) than less silicic granitic rocks, for which the reasons are unclear. Here we report Zn isotopic data for leucosomes (L, melt) and melanosomes phases (M, residue) in migmatites as well as granitoids from the Dabie orogenic belt, central China. Leucosomes always have higher $\delta^{66}Zn$ than their associated melanosomes, with $\Delta^{66}Zn_{L-M}$ ($\delta^{66}Zn_L - \delta^{66}Zn_M$) varying widely from 0.08‰ ± 0.07‰ to 0.76‰ ± 0.07‰. High $(Th/U)_{L/M}$ ($\frac{(Th/U)leucosome}{(Th/U)melanosome}$) ratios of four migmatite samples indicate modification of the leucosomes by fluid exsolution. Rayleigh fractionation modeling suggests that fluid exsolution could be responsible for the elevated $\delta^{66}Zn$ in the four leucosomes. Three samples with large $\Delta^{66}Zn_{L-M}$ values and positive Eu anomalie, also have high $\Delta^{66}Zn_{L\text{-}M}$ values, probably due to accumulation of isotopically heavy plagioclase. Equilibrium Zn isotopic fractionation caused by partial melting is modeled to be 0.14‰–0.18‰ ($\Delta^{66}Zn_{melt-residual}$) at 704–820 °C, consistent with the measured diatexite data ($\Delta^{66}Zn_{L\text{-}M}$ = 0.14‰ ± 0.07‰). The remaining two samples that were not significantly affected by fluid exsolution or plagioclase accumulation yield $\Delta^{66}Zn_{L\text{-}M}$ values larger than those expected in equilibrium melting and may reflect disequilibrium fractionation between melt and residue during the rapid melt segregation from the source. Our study confirms that Zn isotopes could be significantly fractionated during crustal anatexis and the magnitude of fractionation can be further enhanced by late-stage magmatic differentiation. Therefore, zinc isotope may act as a potential indicator of crust differentiation.

1. Introduction

High-silica granitic rocks (SiO_2 > 70 wt%) commonly exhibit larger isotopic variations (e.g. Fe, Mg, Si, and Li) than more mafic rocks (Foden et al., 2015; Savage et al., 2011, 2012; Sossi et al., 2012; Telus et al., 2012; Xu et al., 2017; Zambardi et al., 2014; Zhu et al., 2015 and references therein). The Fe isotopic variations in high-silica granitic rocks have been inferred to result from fluid exsolution, which removes isotopically light Fe and increase the $\delta^{56}Fe$ values of high-silica granitic rocks (Heimann et al., 2008; Poitrasson and Freydier, 2005), the fractional crystallization of titanomagnetite (Schuessler et al., 2009), partial melting (Telus et al., 2012; Xu et al., 2017), source heterogeneity (He et al., 2017), diffusion (Teng et al., 2011; Zambardi et al., 2014), and high melt oxygen fugacity (Foden et al., 2015; Sossi et al., 2012).

Zinc (Zn) is a trace element in the continental crust and mantle (crust: ~72 ppm; mantle: ~55 ppm; McDonough and Sun, 1995; Rudnick and Gao, 2003). In compounds or complexes, Zn has only one valence state (Zn^{2+}) and is thus insensitive to changes in redox conditions. Despite this, large Zn isotopic variations (0.12‰ to 0.88‰) have been observed in felsic rocks (Doucet et al., 2018; Huang et al., 2018b; Telus et al., 2012; Xia et al., 2017). Pegmatites from Black Hills, South Dakota (USA), are the isotopically heaviest terrestrial igneous rocks reported so far with $\delta^{66}Zn$ values of +0.53‰ to +0.88‰ (Telus et al., 2012). The heavy Zn isotopic compositions of pegmatites have been attributed to fluid exsolution during the late stages of granitic magma evolution. In addition to pegmatites, granitoids also have a wide range of $\delta^{66}Zn$ values from 0.12‰ to 0.49‰ (Doucet et al., 2018; Telus et al., 2012).

The higher $\delta^{66}Zn$ values of high-silica granitic rocks relative to less-silica granitic rocks are shown in Fig. 1. However, the cause for this difference is debated. Chen et al. (2013) suggested that Zn isotope fractionation caused by fractional crystallization is <0.1‰ based on analysis of a suite of cogenetic samples from Kilauea Iki. Recently, several studies have proposed that Zn isotopes can be significantly fractionated during mantle melting, given the Zn isotope difference between basalts and refractory peridotites, which is interpreted to preferential consumption of spinel (Wang et al., 2017), or isotope fractionation

* Corresponding author.
E-mail addresses: xulj@cugb.edu.cn (L.-J. Xu), lsa@cugb.edu.cn (S.-A. Liu).

https://doi.org/10.1016/j.lithos.2018.11.028
0024-4937/

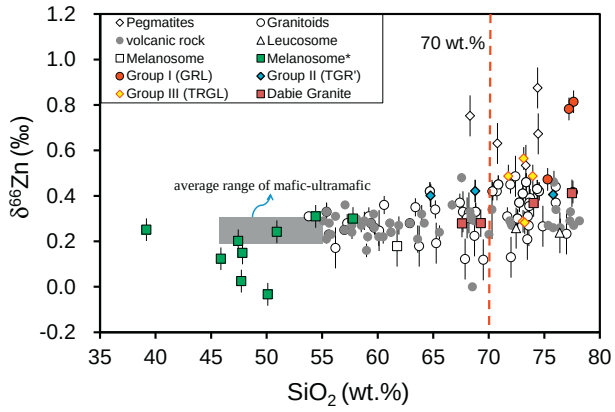

Fig. 1. δ^{66}Zn versus SiO_2 (wt.%) diagram for pegmatites, granitoids. Data of δ^{66}Zn and SiO_2 for pegmatites (white diamond), migmatite (grey triangle-melanosome and grey square-leucosome) are from Telus et al. (2012). Data of δ^{66}Zn and SiO_2 for granitoids (white circle), mafic-ultramafic rocks, volcanic rocks (grey circle) are from Telus et al. (2012), Chen et al. (2013), Laurent et al. (2014), Xia et al. (2017), Doucet et al. (2018) and Huang et al. (2018a, 2018b). Data of δ^{66}Zn for the melanosome (green square), Group I (red circle), Group II (blue diamond), Group III (yellow diamond) leucosome and Dabie granite (red square) are from this study, and data of SiO_2 for the Dabie pegmatite and granite are from Wang et al. (2013) and He et al. (2011), respectively. (For interpretation of the references to colour in this figure legend, the reader is referred to the web version of this article.)

between melts and residual minerals (Sossi et al., 2018). Recently, Doucet et al. (2018) suggest that partial melting of ancient felsic crust might cause Zn isotope fractionation of up to +0.15‰ due to disequilibrium kinetic fractionation. Migmatites are generated by partial melting of the continental crust, which is ceased during forming granite. Thus, migmatites may provide an opportunity to access the mechanism of Zn isotopic fractionation during fractional crystallization, fluid exsolution, especially for crustal partial melting.

Migmatites are formed by the decomposition of hydrous minerals (e.g.,muscovite, biotite, and amphibole) under fluid-absent (at high temperature) or fluid-present (at low temperature) conditions in the continental crust (Brown, 2007; Sawyer et al., 2011). Typically, migmatites contain leucosomes (igneous rocks) and melanosomes (metamorphic rocks), that are petrogenetically related to each other (Sawyer et al., 2011; Xu et al., 2013). In situ zircon U—Pb dating, mineralogy composition and the detail zone textures, major–trace element and oxygen isotope for different types of garnets from leucosome and melanosome suggest they are from the same protoliths (Brown, 2001; Xu et al., 2013). In most cases, one of the partially melted phases in a migmatite, which contains high-silica granitic assemblages (e.g., feldspar and quartz), would form light-colored leucosomes. The other phase is typically residual solid materials (e.g., amphibole and biotite), which forms dark-colored melanosomes. Therefore, leucosomes and melanosomes in migmatites could be utilized to investigate isotope fractionation during crustal melting. To date, only three migmatite samples (two leucosomes and one melanosome) from the Black Hills have been analyzed (Telus et al., 2012), revealing that the leucosome has slightly higher δ^{66}Zn than their associated melanosome. It should be noted that leucosomes commonly experience multiple processes during or after formation, including partial melting, fractional crystallization, and fluid exsolution (e.g., Sawyer et al., 2011; Xu et al., 2017). All of these processes have the potential to modify Zn isotopic ratios of leucosomes.

In this study, we report high-precision Zn isotopic data for well-characterized migmatites and granitoids with the same protolith source from the Dabie orogen, central China. These data are used to assess the Zn isotope fractionation behaviors during a series of processes including fluid activity, plagioclase accumulation, fractional crystallization, and crustal melting in the Dabie migmatite (Wang et al., 2013). The granitoids have a wide range of SiO_2 contents (He et al., 2011, 2013; Wu et al., 2017), and this enables an assessment of whether the Zn isotopic ratios of high-silica granites shift to heavier values with increasing SiO_2 contents. Integration of our new Zn isotopic data with existing mineralogical, petrologic, and geochemical data provides new insights into the mechanisms of Zn isotope fractionation in high-silica igneous rocks.

2. Geological setting and sample description

2.1. Geological setting

The Dabie–Sulu orogenic belt was formed by the Triassic continental collision between the North China Craton (NCC) and South China Craton (SCC) (e.g., Cong, 1996; Li et al., 1993) (Fig. 2). The Dabie orogen is divided into a series of fault-bounded metamorphic zones, based on their different mineralogy, petrology, geochemistry and P-T-t evolution of metamorphic rocks (e.g. Li et al., 2001; Xu et al., 1992). In general, from south to north, it comprises the Susong High Pressure Metamorphic Zone (HPZ), the South Dabie Terrane (SDT), the Central Dabie midium-T/ ultrahigh-pressure Terrane (CDT), the North Dabie Terrane (NDT), and the North Huaiyang Zone (NHY). The SDT is located in the south, and is bounded by the Huangliangting–Mituo Fault to the north and Taihu–Mamiao Fault to the south. The CDT is bounded by the Wuhe–Shuihou Fault to the north and the Huangliangting–Mituo Fault to the south. The peak UHP metamorphic Sm—Nd isochron ages of the CDT are ca. 229–226 Ma (Li et al., 2000). The NDT is located in the north of the Dabie orogen, bounded by the Xiaotian–Mozitan Fault to the north and the Wuhe–Shuihou Fault to the south. Dioritic to granodioritic orthogneiss, eclogitic amphibolite, granulite, retrograded eclogite, and garnet pyroxenite crop out widely throughout this area (e.g. Li et al., 2005 and references therein). The ultrahigh pressure (UHP) peak metamorphic age for the NDT is ca. 224 Ma, as evidenced by abundance UHP metamorphic evidences (e.g., diamond and coesite inclusions) and Triassic metamorphic ages (Li et al., 1993; Liu et al., 2010a, 2010b and references therein). The NDT experienced amphibolite-facies retrograde metamorphism during 200–180 Ma (Liu et al., 2010a, 2010b). Post-collisional magmatism was widespread in the Dabie orogenic belt during the Early Cretaceous, as represented by numerous granitoid plutons with intrusion ages of 143–117 Ma (He et al., 2011; Huang et al., 2008; Wang et al., 2007)

2.2. Migmatites of the Dabie orogen

A total of 22 migmatite samples (8 melanosomes, 2 amphibolitic schollens and 12 leucosomes) from the NDT were selected for analysis in this study: 14 samples from Manshuihe, 4 samples from Qingtian, and the another 4 are from Baojia and Guofouan (Fig. 2). These migmatites vary from metatexite to diatexite with increasing degree of metamorphism. The metatexites are characterized by a patchy or layered structure (Fig. 3a). Amphibolitic schollens (Fig. 3b) from the melanosomes in the diatexites, are amphibolitic blocks. The detailed petrology, geochronology, and geochemistry of these migmatites have been previously characterized by Wang et al. (2013). The migmatization protoliths were migmatized at 128–135 Ma based on U—Pb dating. The migmatites are thought to have been produced by fluid-present melting of intermediate to felsic protoliths (dioritic to granodioritic gneisses) at $P = 5$–7 kbar and $T = 700$–800 °C (Wang et al., 2013). The diatexites of this study are also mainly from Qingtian, which is closer to the Yuexi dome than to the Manshuihe (Fig. 2). Previous studies have suggested that the diatexitic leucosomes near the Luotian dome formed at temperature of 760–820 °C (Wang, 1991; Wang et al., 1997), which is slightly higher than the temperature (705–744 °C) calculated from matrix plagioclase and amphibole for the Manshuihe metatexites (Wang et al., 2013). Melanosome rims adjacent to the leucosomes are typically characterized by large and euhedral amphibole grains (Fig. 3d). In addition, poikilitic and porphyritic amphiboles in diatexitic leucosomes suggest that they are peritectic phases in the melting reaction (Sawyer et al., 2011; Wang et al., 2013). Amphibole in melanosomes has higher

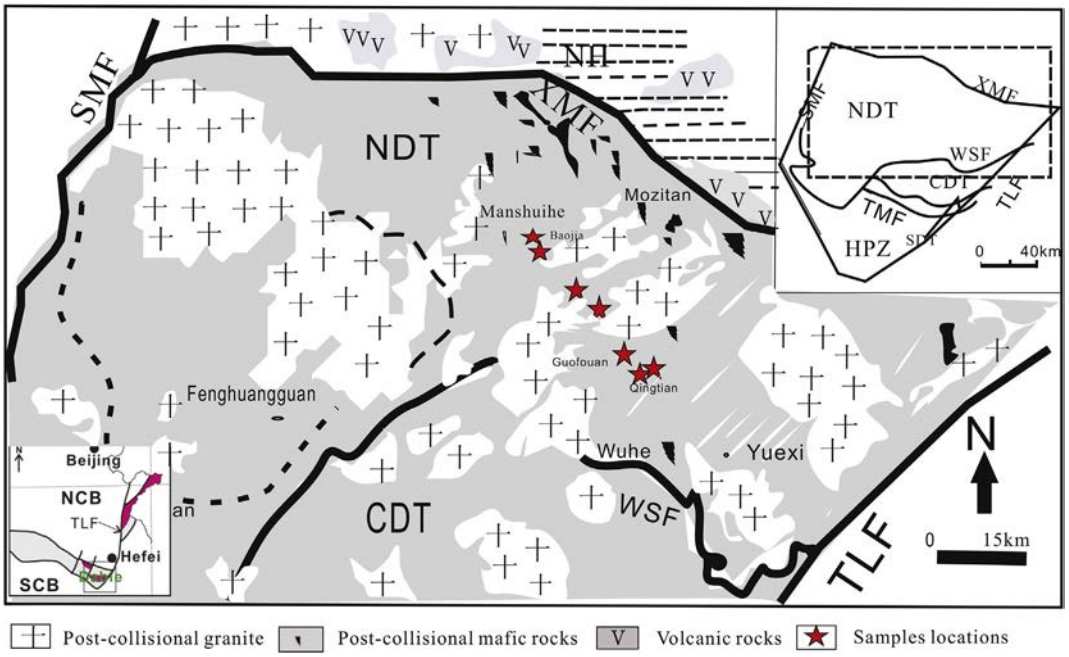

Fig. 2. Simplified geological map of the North Dabie ultrahigh-pressure (UHP) metamorphic terrane, modified after Wang et al. (2013) and He et al. (2011). Abbreviations are as follows: Xiaotian–Mozitan Fault (XMF), North Huaiyang Terrane (NHT), North Dabie Terrane (NDT), Central Dabie medium-T/UHP Terrane (CDT), South Dabie Terrane (SDT), and Susong High Pressure Metamorphic Zone (HPZ). The map at upper right shows the location of the Dabie Orogen. Sample localities are labeled as red stars: 14 samples are from Manshuihe; 4 from Qingtian; and 4 in total from Baojia and Guofouan, (red stars between Manshuihe and Qingtian). (For interpretation of the references to colour in this figure legend, the reader is referred to the web version of this article.)

MgO and lower FeO contents than the peritectic amphibole in the leucosomes. Rounded inclusions of plagioclase, quartz, and/or biotite are commonly present in peritectic amphiboles of leucosomes, suggesting a reaction of plagioclase + quartz + biotite is involved in producing the amphibole. Furthermore, plagioclase in melanosomes has higher anorthite contents than that in the leucosomes (An = 30.5 ± 2.5 versus An = 28.3 ± 1.5, respectively), suggesting that plagioclase in the melanosome is a residual phase during partial melting. The influx of a mixed $H_2O + CO_2$ fluid has been proposed, based on the presence of calcite in the melanosomes (0907MSH-1A) with high loss-on-ignition (LOI; 9.9 wt%) values and CaO contents (24.9 wt%). Thus, the melting reaction can be expressed as follows:

$$\text{biotite} + \text{plagioclase} + \text{quartz} + \text{fluid} \rightarrow \text{granitic melt} + \text{amphibole} + \text{residual plagioclase}$$

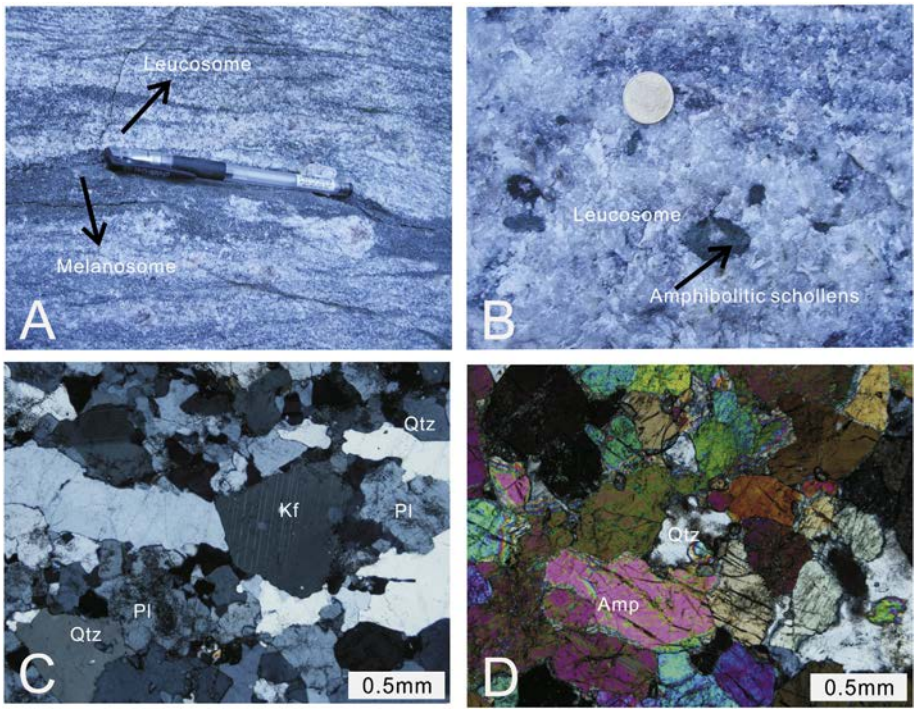

Fig. 3. (a) Layered structure of the metatexitic migmatites. (b) Amphibolitic schollens in the diatexitic migmatites. (c) Equant subhedral to euhedral plagioclase and quartz in the Group III leucosomes. (d) Euhedral amphibole in a melanosome. pl = plagioclase; Amp = amphibole; Kf = K-feldspar; Qtz = Quartz.

The leucosomes in the migmatites are divided into three groups according to La/Yb and Sr/Y ratios, and chondrite-normalized rare earth element (REE) patterns (Fig. 4). Group I are granitic leucosomes (GRL: the abbreviation of granitic leucosomes, Metatexites, 4 samples), which are fine-grained and typically have stromatic structures. The GRL are composed of plagioclase (10%–20%), K–feldspar (10%–20%), quartz (60%–70%), biotite + amphibole (1%–5%), and accessory zircon, titanite and Fe-oxides. These leucosomes have high La/Yb_N (chondrite-normalized La/Yb) ratios of 109.3–141.7 and moderate Sr/Y ratios of 54–76 (Fig. 4a). The GRL and associated melanosomes in metatexites preserve obvious coherent pre–partial melting structures, such as layering and foliation structures. The layered structures of Group I leucosomes indicate a local derivation that was either in-situ or within-source (Sawyer, 2008). Group II (GRL'; diatexites; $n = 3$) represent melts + peritectic amphiboles. The GRL' contain peritectic amphiboles and have low $(La/Yb)_N$, low Sr/Y ratios, and flat chondrite-normalized heavy REE patterns ($(La/Yb)_N = 4.32–13.7$; $Sr/Y = 25–71$) (Fig. 4b). These leucosomes and melanosomes from the diatexites are in an advanced stage of anatexis (Ashworth, 1985; Wimmenauer and Bryhni, 2002 and references therein). Group III leucosomes are trondhjemitic leucosomes (TRGL; metatexites; $n = 5$), and are composed mainly of quartz (45%–60%), plagioclase (35%–50%), K–feldspar (1%–5%), and biotite (<1%), with minor zircon, titanite and Fe oxides. Group III leucosomes have cumulate textures comprising plagioclase and quartz with subhedral to euhedral shapes (Fig. 3c). The TRGL have high $(La/Yb)_N = 16–18$ and $Sr/Y = 308–1735$ (except 0907MSH–4b) values and show prominent positive Eu* ($Eu_N/\sqrt{(Sm_N \times Gd_N)}$) anomalies (Fig. 4c).

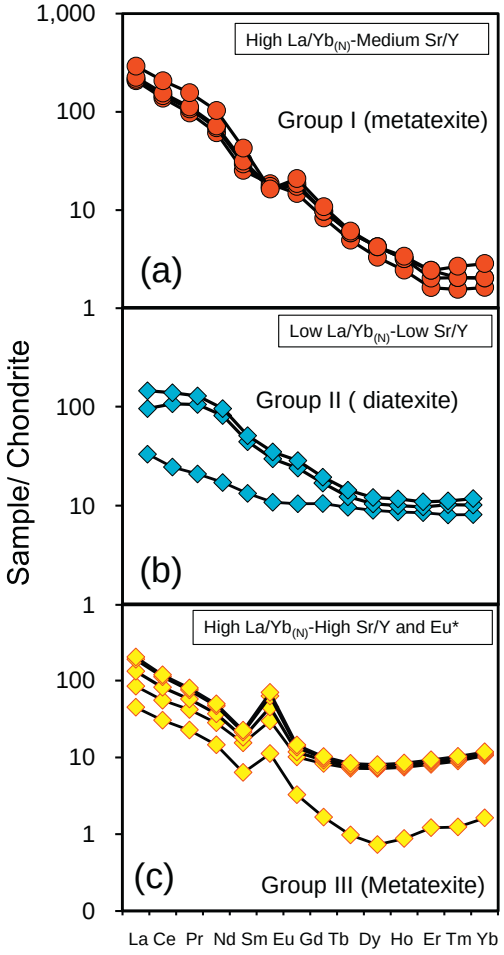

Fig. 4. Chondrite-normalized REE patterns for the three groups of leucosomes from the Dabie migmatites. Chondrite values are from McDonough and Sun (1995). The Group I (from metatexites) leucosomes have high $(La/Yb)_N$ and moderate Sr/Y ratios. The Group II leucosomes (from diatexites) have low $(La/Yb)_N$ and low Sr/Y ratios, and flat heavy REE patterns. The Group III leucosomes (from metatexites) have high $(La/Yb)_N$ and Sr/Y ratios (except 0907MSH-4b), and prominent positive Eu anomalies.

Melanosomes from the metatexites in contact with Group I and III leucosomes are composed mainly of biotite (30%–40%), plagioclase (10%–30%), amphibole (35–45%), quartz (5%–10%), and K-feldspar (0%–5%). Melanosomes from diatexites in contact with Group II leucosomes have been pervasively infiltrated by small leucogranitic patches. The SiO_2 contents of amphibolitic schollens range from 50.9 wt% (0907-QT-1-A) to 57.8 wt% (0907-QT-4-A).

In general, the studied leucosomes and melanosomes are in direct contact with each other, and thus defined melanosome–leucosome pairs that were evident in the field. For some migmatites, e.g., 0907-MSH-5 and 0907-MSH-5′, two different types of leucosomes (Group I and III) co-exist in a single specimen scale.

2.3. Granites and orthogneisses of the Dabie orogen

The protoliths of the Dabie migmatites analyzed here are mainly orthogneisses, which are widespread in the Dabie Orogen, central China (Wang et al., 2013). Two orthogneisses from the NDT and four granites from the NHY and HPZ were also analyzed for Zn isotopes. The petrology, geochronology and geochemistry of two granodioritic gneisses (12-DB-37 and12-DB-38) have been described in Xia et al. (2016). The metamorphic ages of the two granitic orthogneisses in this region are ~240 Ma and ~220 Ma, respectively (Zheng et al., 2005). The granitic orthogneisses mainly comprise quartz, K-feldspar, plagioclase, and minor biotite, muscovite, garnet, phengite, and epidote/allanite. They experienced the same UHP metamorphic evolution as the eclogite units (Carswell et al., 2000; Liu et al., 2001). The detailed petrology, geochronology and geochemistry of four granites (06HSW-2; 07YC-3; 07LD-2 and 07SJS-2) have been described by He et al. (2011, 2013). The intrusion ages for these granitoids are <130 Ma (He et al., 2011 and references therein). These are Early Cretaceous post-collisional, I-type, non-adakitic granitoids with a wide range of SiO_2 contents (69.3–77.5 wt%), and they contain mainly quartz, K-feldspar, plagioclase, biotite, and/or amphibole (He et al., 2011, 2013; Wu et al., 2017).

3. Analytical methods

Zinc isotopic analyses were carried out in the Isotope Geochemistry Laboratory of the China University of Geosciences, Beijing, China. The detailed procedures for column chemistry and mass spectrometry have been reported in previous studies (Liu et al., 2014, 2016; Lv et al., 2016; Huang et al., 2016); consequently, only a brief description is provided here. Sample powders (20–60 mg) were completely dissolved in $HF–HNO_3–HCl$ acids. Zinc was purified with 2 ml of pre-cleaned AG-MP-1 M resin (Bio-Rad strong anion exchange resin). The matrix was removed by eluting 8 N HCl and 2 N HCl, and Zn was collected in the final 10 ml of 0.5 N HNO_3. The total procedure blank for Zn is <6 ng, which is negligible compared with the total amount of processed Zn (> 400 ng). The potential presence of matrix elements (Mg and Al) was checked prior to isotopic ratio measurement, as the presence of Mg and Al can produce molecular interferences ($^{27}AlAr^+$, $^{24}MgAr^+$ and $^{26}MgAr^+$) and compromise Zn isotopic measurements (Liu et al., 2016; Mason et al., 2004). The purified Zn solution was dried down, and then dissolved in 3% HNO_3 for isotopic analysis using a Thermo-Finnigan Neptune Plus multiple–collector inductively coupled plasma mass spectrometer (MC–ICP–MS). Sample–standard bracketing was used for instrumental mass bias correction. High-sensitivity (X) cones were used to ensure that the ^{66}Zn signal intensity was around ~1.5 V for a 200 ppb Zn solution. Each sample was analyzed three times for

40 cycles/each time in low-resolution mode using a wet plasma. The measured Zn isotopic data are reported in δ-notation form in per mil relative to JMC 3-0749L:

$$\delta^{66,68}\mathrm{Zn}\ (‰) = \left(\left(^{66,68}\mathrm{Zn}/^{64}\mathrm{Zn}\right)_{\mathrm{sample}}/\left(^{66,68}\mathrm{Zn}/^{64}\mathrm{Zn}\right)_{\mathrm{JMC\ 3-0749L}} - 1\right) \times 1000$$

The international basalt standards BHVO-2 and BCR-2 were analyzed to assess data accuracy (Table 1). The obtained values ($\delta^{66}\mathrm{Zn}_{\mathrm{BHVO\text{-}2}} = 0.31‰ \pm 0.05‰$ and $\delta^{66}\mathrm{Zn}_{\mathrm{BCR\text{-}2}} = 0.30‰ \pm 0.05‰$) are identical within external uncertainties with those of previous studies (Liu et al., 2014, 2016; Sossi et al., 2015; Wang et al., 2017; Huang et al., 2016, 2018a, 2018b; Xia et al., 2017). The external reproducibility for δ^{66}Zn was better than ±0.05‰ (2SD) based on long-term analyses of the international Zn standard solution IRMM 3702 (0.27 ± 0.03‰; n = 47; 2SD) and basalt standard BHVO-2 (0.31‰ ± 0.05‰; n = 22; 2SD) over a period of two years (Liu et al., 2016, 2017). All uncertainties are given as 2SD, unless stated otherwise.

The Zn concentrations for plagioclase, K-feldspar and biotite were analyzed using an Element XR ICP-MS in the Isotope Geochemistry Laboratory of China University of Geosciences, Beijing. International rhyolite and granite standards (AGV-2 and GSP-2) were analyzed to assess data accuracy. The Zn concentrations obtained for AGV-2 and GSP-2 were 76.17 ppm and 98.12 ppm, respectively, which are identical with the recommend values (https://crustal.usgs.gov/ geochemical_reference_standards/) within external uncertainties (≤10%). The analytical precision and accuracy (1σ) for Zn concentration are better than ±5%.

4. Results

Zinc isotope data obtained in this study are listed in Table 1. The δ^{66}Zn values vary from −0.03‰ ± 0.05‰ to 0.27‰ ± 0.05‰ for melanosomes and from 0.28‰ ± 0.05‰ to 0.81‰ ± 0.05‰ for leucosomes (Fig. 5), with an overall variation of up to 0.84‰. Group I, II and III leucosomes have δ^{66}Zn values from 0.42‰ ± 0.05‰ to 0.81 ± 0.05‰, from 0.40‰ ± 0.05‰ to 0.42‰ ± 0.05‰, and from 0.28‰ ± 0.05‰ to

Table 1
The δ^{66}Zn, δ^{68}Zn (‰) and $\Delta^{66}\mathrm{Zn}_{\mathrm{L\text{-}M}}$ values for the Dabie migmatite, granites and orthogneisses.

Sample	Type	Classification	δ^{66}Zn	2SD	δ^{68}Zn	2SD	n	$\delta^{66}\mathrm{Zn}_{\mathrm{L}}$-$\delta^{66}\mathrm{Zn}_{\mathrm{M}}$	2SD
Patch metaexite									
09GFA-2-A	Melanosome		0.20	0.05	0.40	0.10	3		
09GFA-2-B	Leucosome	Group III (Cumulates)	0.28	0.05	0.56	0.10	3	0.08	0.07
Stromatic metatexite									
0907MSH-1-A	Melanosome		0.25	0.05	0.52	0.10	3		
0907MSH-1-B	Leucosome	Group III (Cumulates)	0.56	0.05	1.11	0.10	3	0.31	0.07
0907MSH-4-A	Melanosome		−0.02	0.05	−0.05	0.10	3		
Repeat			−0.04	0.05	−0.08	0.10	3		
Average			−0.03	0.07	−0.07	0.14	3		
0907MSH-4-B	Leucosome	Group III (Cumulates)	0.29	0.05	0.57	0.10	3	0.32	0.09
0907MSH-5-A	Melanosome		0.12	0.05	0.24	0.10	3		
Repeat			0.18	0.05	0.36	0.10	3		
Average			0.15	0.07	0.30	0.14	3		
0907MSH-5-A	amphibole		0.16	0.05	0.24	0.10	3		
0907MSH-5-A	biotite		0.15	0.05	0.22	0.10	3		
0907MSH-5-A	Fe-oxide		0.21	0.05	0.33	0.10	3		
0907MSH-5-B	Leucosome	Group III (Cumulates)	0.49	0.05	0.97	0.10	3	0.34	0.09
0907MSH-5-C	Leucosome	Group I (melts)	0.81	0.05	1.63	0.10	3	0.66	0.09
0907MSH-5-A1	Melanosome		0.03	0.05	0.06	0.10	3		
0907MSH-5-B1	Leucosome	Group III (Cumulates)	0.49	0.05	0.99	0.10	3	0.46	0.07
0907MSH-5-C1	Leucosome	Group I (melts)	0.78	0.05	1.53	0.10	3	0.76	0.07
0907MSH-6-A	Melanosome		0.12	0.05	0.24	0.10	3		
0907MSH-6-C	Leucosome	Group I (melts)	0.47	0.05	0.93	0.10	3	0.35	0.07
0907MSH-7-A	Melanosome		0.31	0.05	0.62	0.10	3		
0907MSH-7-C	Leucosome	Group I (melts)	0.42	0.05	0.83	0.10	3	0.11	0.07
Diatexite									
0907BJ-2-A	Melanosome		0.27	0.05	0.52	0.10	3		
0907BJ-2-B	Leucosome	Group II (Melts″)	0.41	0.05	0.79	0.10	3	0.14	0.07
0907QT-1-A	Melanosome		0.21	0.05	0.41	0.10	3		
Repeat			0.28	0.05	0.56	0.10			
Average			0.24	0.07	0.48	0.14			
0907QT-4-A	Amphibolitic Schollen		0.20	0.05	0.39	0.10	3		
Repeat			0.30	0.05	0.58	0.10			
Average			0.25	0.07	0.49	0.14			
0909QT-4	Leucosome	Group II (Melts″)	0.42	0.05	0.83	0.10	3		
0909QT-2-B	Leucosome	Group II (Melts″)	0.40	0.05	0.78	0.10	3		
07-sjs-2	Dabie granite		0.37	0.05	0.71	0.11	3		
0909QT-2-B	Leucosome	Group II (Melts″)	0.40	0.05	0.78	0.10	3		
07-sjs-2	Dabie granite		0.37	0.05	0.71	0.11	3		
06-hsw-2	Dabie granite		0.41	0.05	0.79	0.11	3		
07LD-2	Dabie granite		0.28	0.05	0.53	0.11	3		
07yc-3	Dabie granite		0.28	0.05	0.51	0.11	3		
12-DB-37	Dabie orthogneisses		0.27	0.05	0.54	0.11	3		
12-DB-38	Dabie orthogneisses		0.24	0.05	0.43	0.11	3		
Geostandards									
BHVO-2			0.31	0.05	0.61	0.10	3		
BCR-2			0.30	0.05	0.60	0.10	3		

The melanosome and leucosome from the same rock have same sample labels, e.g., 0907MSH-7-A(melanosome) and 0907MSH-7-C(leucosome). Two standard deviation (2SD) for the $\delta^{66}\mathrm{Zn}_{\mathrm{L}}$-$\delta^{66}\mathrm{Zn}_{\mathrm{M}}$ (‰) is calculated by $\sqrt{(2 * SD_L{}^2 + 2 * SD_M{}^2}$.

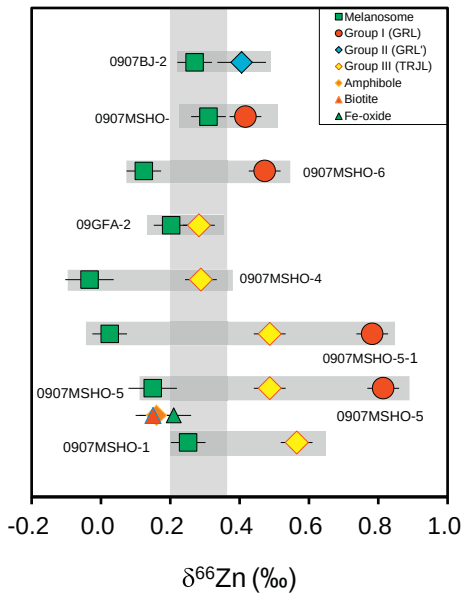

Fig. 5. $\delta^{66}Zn$ values for different melanosome–leucosome pairs (grey bars), and biotite, amphibole, and Fe—Ti oxide minerals in the melanosome (0907 MSH-5). The grey bar denotes the $\delta^{66}Zn$ value of basalt ($\delta^{66}Zn_{basalt}$ = 0.28‰ ± 0.05‰; 2SD; Chen et al., 2013; Wang et al., 2017).

0.56‰ ± 0.05‰, respectively (Figs. 5–6). In all samples, leucosomes have higher $\delta^{66}Zn$ values than the spatially associated melanosomes (Fig. 5). The $\delta^{66}Zn$ values for granitic leucosomes (Group I) are slightly higher than those for the other two groups (Group II and III).

The apparent isotopic offset between each leucosome and its spatially-associated melanosome is expressed as $\Delta^{66}Zn_{L-M}$ ($\delta^{66}Zn_L - \delta^{66}Zn_M$) and listed in Table 1. The leucosome–melanosome pairs of Groups I and Group III have $\Delta^{66}Zn_{L-M}$ values varying from 0.11‰ ± 0.07‰ to

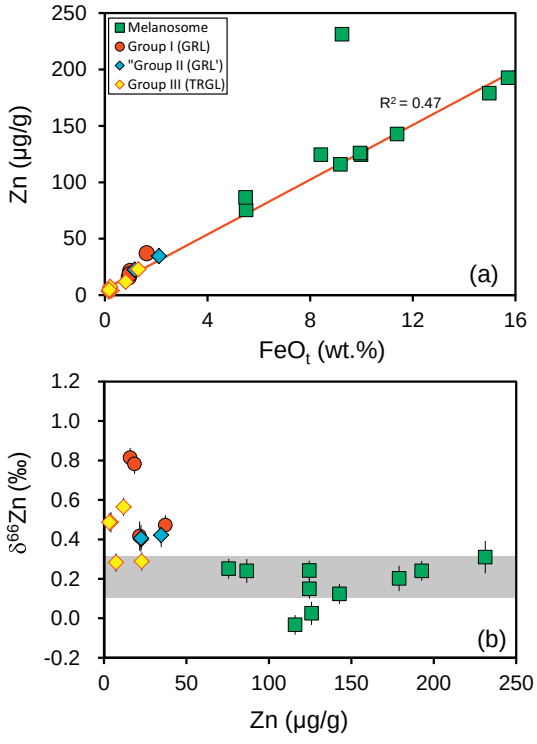

Fig. 6. (a) Zn versus FeOt and (b) $\delta^{66}Zn$ versus Zn diagrams for different melanosomes and leucosomes from the Dabie migmatites. Symbols are as in previous figures.

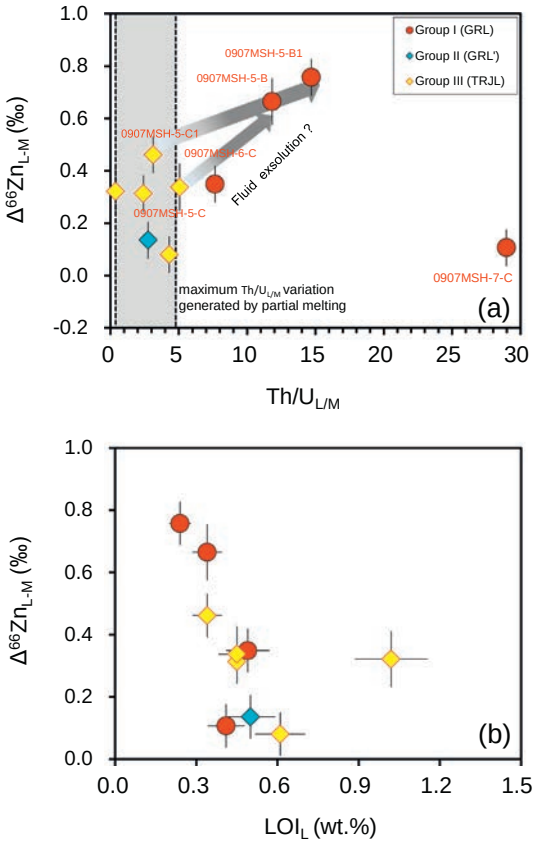

Fig. 7. (a) Plot of $\Delta^{66}Zn_{L-M}$ versus $Th/U_{L/M}$. "L" and "M" indicate leucosome and melanosome, respectively. "$\Delta^{66}Zn_{L-M}$" denotes the isotopic difference between a leucosome and associated melansome (i.e., $\delta^{66}Zn_{leucosome} - \delta^{66}Zn_{melanosome}$). The grey arrows indicate that two types of leucosome (Group I and III) co-exist in a hand specimen (e.g., 0907 MSH-5-B and 0907 MSH-5-C). In such samples, one type of leucosome has high $Th/U_{L/M}$ and $\Delta^{66}Zn_{L-M}$ (Group I), and the other has low $Th/U_{L/M}$ and $\Delta^{66}Zn_{L-M}$, suggesting the influence of fluid exsolution. (b) Plot of $\Delta^{66}Zn_{L-M}$ versus LOI values for different leucosomes.

0.76‰ ± 0.07‰ and from 0.08‰ ± 0.07‰ to 0.46‰ ± 0.07‰, respectively (Fig. 7). Only one Group II leucosome–melanosome pair was analyzed ($\Delta^{66}Zn_{L-M}$ = 0.14‰ ± 0.07‰). Overall, the $\Delta^{66}Zn_{L-M}$ values of all samples obtained in this study are much higher than the range reported for migmatites from Black Hills (0.06‰ ± 0.09‰, Telus et al., 2012).

Amphibole, biotite and Fe oxides from a melanosome (0907-MSH-5-A) have $\delta^{66}Zn$ values of 0.16‰ ± 0.05‰, 0.15‰ ± 0.05‰ and 0.21‰ ± 0.05‰, respectively (Fig. 5). Two amphibolitic schollens in the diatexitic melanosome have identical $\delta^{66}Zn$ values of 0.25‰ ± 0.07‰ (0907-QT-4-A) and 0.24‰ ± 0.07‰ (0907-QT-1-A), respectively. The four granites (06HSW-2; 07YC-3; 07LD-2; 07SJS-2) have $\delta^{66}Zn$ values varying from 0.28‰ ± 0.05‰ to 0.41‰ ± 0.05‰ (Fig. 1). Two orthogneisses (12-DB-37, 12-DB-38) from the Dabie orogenic belt have similar $\delta^{66}Zn$ values (0.24‰ ± 0.05‰ and 0.27 ± 0.05‰) (Table 1). The Zn concentrations for plagioclase (0907-MSH-5B, leucosome), K-feldspar (0907-MSH-5B; leucosome) and biotite (0907-MSH-5A; melanosome) are 2.55 ppm, 1.02 ppm, and 198.69 ppm, respectively (Table 2).

Table 2
Parameters used in modeling of Zn isotope fractionation during plagioclase accumulation.

Zn_{pl} (ppm)	$\delta^{66}Zn_{pl}$ (‰)	Zn_{bio} (ppm)	$\delta^{66}Zn_{bio}$ (‰)	f_{bio} (%)	Zn_L (ppm)	$\delta^{66}Zn_L$ (‰)	$\delta^{66}Zn_M$ (‰)	ΔZn_{L-M} (‰)
2.55	0.55	198.69	0.15	0.3	3.14	0.47	0.03	0.44
				0.5	3.53	0.44	0.10	0.34
				2.5	7.45	0.28	0.20	0.08

Note: pl-plagioclase; bio-biotite; f_{bio}-modal proportion of biotite in the leucosome; L-leucosome; M-melanosome

5. Discussion

To avoid the influence of protolith heterogeneity on the Zn isotopic systematics of migmatites, $\Delta^{66}Zn_{L-M}$ values for melanosome–leucosome pairs, rather than $\delta^{66}Zn$ values of leucosomes, are considered in the following discussion. An obvious feature is the large variation in apparent Zn isotopic fractionation between leucosomes and melanosomes ($\Delta^{66}Zn_{L-M}$ = 0.08‰ to 0.76‰). Telus et al. (2012) reported Zn isotopic data for two migmatites and one melanosome-leucosome pair ($\Delta^{66}Zn_{L-M}$ = 0.06‰ ± 0.09‰). The value they reported is similar to the lowest value observed in the present study. Zinc concentrations generally show a positive correlation with FeO_t (except one sample: 0907MSH-7-A) (Fig. 6a), which indicates that Zn replaces Fe^{2+} and Mg^{2+} and is hosted mainly by ferromagnesian minerals (biotite, amphibole, and Fe oxides). These Zn-bearing minerals in the melanosomes have significantly lighter Zn isotopic compositions (biotite = 0.15‰; amphibole = 0.16‰; Fe-oxides = 0.21‰) than the leucosomes (Fig. 5). Thus, the high $\delta^{66}Zn$ values of the leucosomes may be attributed to partial melting process, which leaves isotopically light biotite, amphibole and Fe-oxides in the residue. However, the formation of migmatites is commonly associated with multiple processes, including plagioclase accumulation, and/or fluid influx and exsolution. Thus, we now assess the influence of each of these processes.

5.1. Fluid activity

Silicate melts typically contain abundant volatiles, mainly H_2O, CO_2, SO_2, HCl, and minor H_2S and CO (Sigurdsson et al., 2015). Volatiles are released via fluid exsolution, when magmas ascend to near surface or experience decompression (Sigurdsson et al., 2015). Given the extremely high $\delta^{66}Zn$ value of pegmatites (Fig. 1), Telus et al. (2012) suggested that Zn isotopes are strongly fractionated during fluid exsolution at the late-stages of magma crystallization. The presence of a small amount of calcites in melanosomes of the Dabie migmatites suggests that influx of $H_2O + CO_2$ fluids triggered partial melting of the protoliths (Wang et al., 2013). However, apart from one melanosome (0907MSH-1A), other leucosomes and melanosomes have low LOI values (<2.0 wt %), indicating that significant fluid exsolution occurred prior to final solidification of the melts. Thus, it is necessary to evaluate the influence of fluid exsolution and influx on Zn isotopic fractionation in the Dabie migmatites.

The Th/U ratio is used as an index to assess influence of fluid exsolution (Fig. 6a), given the higher fluid-mobility of U than Th (Hawkesworth et al., 1997). K-feldspar and zircon fractionation (both have $D_U > 1$ and $D_U > D_{Th}$) can also increase the Th/U ratios of their co-existing magmas (Bea et al., 1994; Rubatto and Hermann, 2007). Residual zircon contents in the melanosomes should be <0.4 wt%, given their measured Zr contents of ≤177 ppm. The abundance of K-feldspar is <5 vol% based on point counting. Using the batch partial melting model of Xu et al. (2017), the highest $(Th/U)_{L/M}$ ratio that can be produced by K-feldspar and zircon fractionation during partial melting of the Dabie migmatites is 4.5. Thus, fluid exsolution is the most likely mechanism for generating the high $(Th/U)_{L/M}$ ratios (8–29) of Group I leucosome–melanosome pairs, which have high $\Delta^{66}Zn_{L-M}$ values of up to 0.76‰ (Fig. 7a). The Group I leucosomes with high $Th/U_{L/M}$ ratios (12–15) also have higher $\Delta^{66}Zn_{L-M}$ values (0.66‰–0.76‰) compared with the Group III trondhjemitic leucosomes ($\Delta^{66}Zn_{L-M}$: 0.34‰–0.46‰) and have low $Th/U_{L/M}$ ratios (3.0–5.1) (Fig. 7a). This difference further suggests that fluid exsolution was an important mechanism responsible for the high $\Delta^{66}Zn_{L-M}$ values of the Group I leucosome–melanosome pairs.

Zinc isotopic exchange between the melt (leucosome) and exsolved vapor (fluid exsolution) during the late stages of magmatic differentiation can be modeled using the Rayleigh fractionation equation:

$$\delta^{66}Zn_{melt}\ (‰) = \left(\delta^{66}Zn_{intial\ melt} + 1000\right) \times f^{(\alpha-1)} - 1000 \quad (1)$$

where α is the Zn isotopic fractionation factor between melt and vapor, and f is the mass fraction of Zn in the remaining melt ($f = F_{melt} \times C_{melt}/C_0$, where C_{melt} is the Zn concentration in the remaining melt, C_0 is the initial Zn concentration in the magma, and F_{melt} is the mass fraction of the remaining melt). The protoliths of the Dabie migmatites are orthogneisses (Wang et al., 2013). Thus, the Zn isotopic composition of one leucosome (this study: 0907BJ-2-B = 0.41‰), which was only affected by partial melting (Section 5.3), was used as the initial melt value. Few studies have investigated the fractionation factor (α) between residue and melt. Zinc prefers tetrahedral coordination in high-silica melts with a low number of non-bridging oxygen per tetrahedral cation (NBO/T ≤ ~0.1), and primarily interacts with oxygen atoms (Kohn and Schofield, 1994). Zinc in zincite (ZnO) is also in tetrahedral coordination and interacts mainly with the oxygen atoms, similar to the coordination in a melt (Ducher et al., 2016, 2018). Thus, the Zn isotopic fractionation factor of zincite was utilized to calculate the fractionation factor (α) between the fluid and melt, which is presumed to be controlled by the coordination number. Studies of natural silicate melts and laboratory experiments have shown that Zn exhibits a marked enrichment in water-rich fluids, and transports Zn in the form of Zn chloride complexes (Zajacz et al., 2008). The Zn isotope fractionation factor between ZnO and $Zn(H_2O)^{2+}$ ($\Delta^{66}Zn_{ZnO\text{-}Zn(H_2O)^{2+}} = 0.000038 \times X^2 + 0.0336X$, $X = 10^6/T^2$ with T in K) can be obtained based on the theoretical calculations of Ducher et al. (2016, 2018) and Fujii et al. (2011), which defined a function of Zn isotopic fractionation between $Zn(H_2O)^{2+}$ and $ZnCl_2/ZnCl^+$ ($\Delta^{66}Zn_{ZnCl_2\text{-}Zn(H_2O)^{2+}} = (-0.0924 \times X - 0.0343)$; $\Delta^{66}Zn_{ZnCl^+\text{-}Zn(H_2O)^{2+}} = (-0.0107 \times X - 0.0002)$, $X = 10^6/T^2$). Thus, the Zn isotope fractionation factor between fluid and melt can be derived as follows:

$$\begin{aligned} 1000 \cdot \ln\alpha &= \Delta^{66}Zn_{fluid\text{-}melt} \\ &= \Delta^{66}Zn_{ZnCl_2/ZnCl^+\text{-}Zn(H_2O)2+} - \Delta^{66}Zn_{ZnO\text{-}Zn(H_2O)2+} \end{aligned} \quad (2)$$

The Zn content in the remaining melt during fluid exsolution can be calculated using a Rayleigh fractionation model:

$$C_{melt}/C_0 = (1 - F_{fluid})(D_{fluid/melt} - 1) \quad (3)$$

where $D_{fluid/melt}$ is the partition coefficient of Zn between fluid and melt, which varies from 8 to 136 in co-existing fluid and glass inclusions in natural samples of silicate melt and fluid inclusions (Zajacz et al., 2008). The $D_{fluid/melt}$ values of 136 and 50 were used to explore the $\delta^{66}Zn_{melt}$ variations during fluid exsolution (Fig. 8a–d). F_{fluid} is the mass fraction of released fluid ($F_{fluid} + F_{melt} = 1$). The $\delta^{66}Zn$ value of melt can be calculated as a function of the mass fraction of released fluid, and Eq. (1) can be expressed as follows:

$$\begin{aligned} \delta^{66}Zn_{melt}\ (‰) = &\left(\delta^{66}Zn_{intial\ melt} + 1000\right) \\ &\times \left[(1 - F_{fluid})(D_{fluid/melt} - 1)\right]^{(\alpha-1)} - 1000 \end{aligned} \quad (4)$$

Given that Zn isotope fractionation increases with decreasing temperature, the $\delta^{66}Zn$ value for the remaining melt after fluid exsolution will also increase with decreasing temperature (Fig. 8a–d). In addition, the $\delta^{66}Zn$ value of the remaining melt will also increase with increasing mass fraction of released fluid (F_{fluid}) (Fig. 7a–b). As discussed by Du et al. (2017), the fluid mass fraction (F_{fluid}) varies from 3% to 6%, depending on the volatile content data for silicic melt inclusions taken from the GEOROC database (http://georoc.mpch-mainz.gwdg.de/georoc/). Therefore, the calculated maximum $\Delta^{66}Zn_{melt}$ value is ~0.7‰ to 0.8‰ at T = 700–800 °C and F_{fluid} = ~7% (Fig. 8a). The magmatic equilibrium temperature for the Dabie migmatites is 705–744 °C, as estimated from co-existing metatexitic amphibole and plagioclase (Wang et al., 2013). The diatexites in the Dabie migmatites were formed at 760–820 °C (Wang, 1991; Wang et al., 1997). Thus, fluid exsolution can account for the high $\Delta^{66}Zn$ values of Group I leucosomes

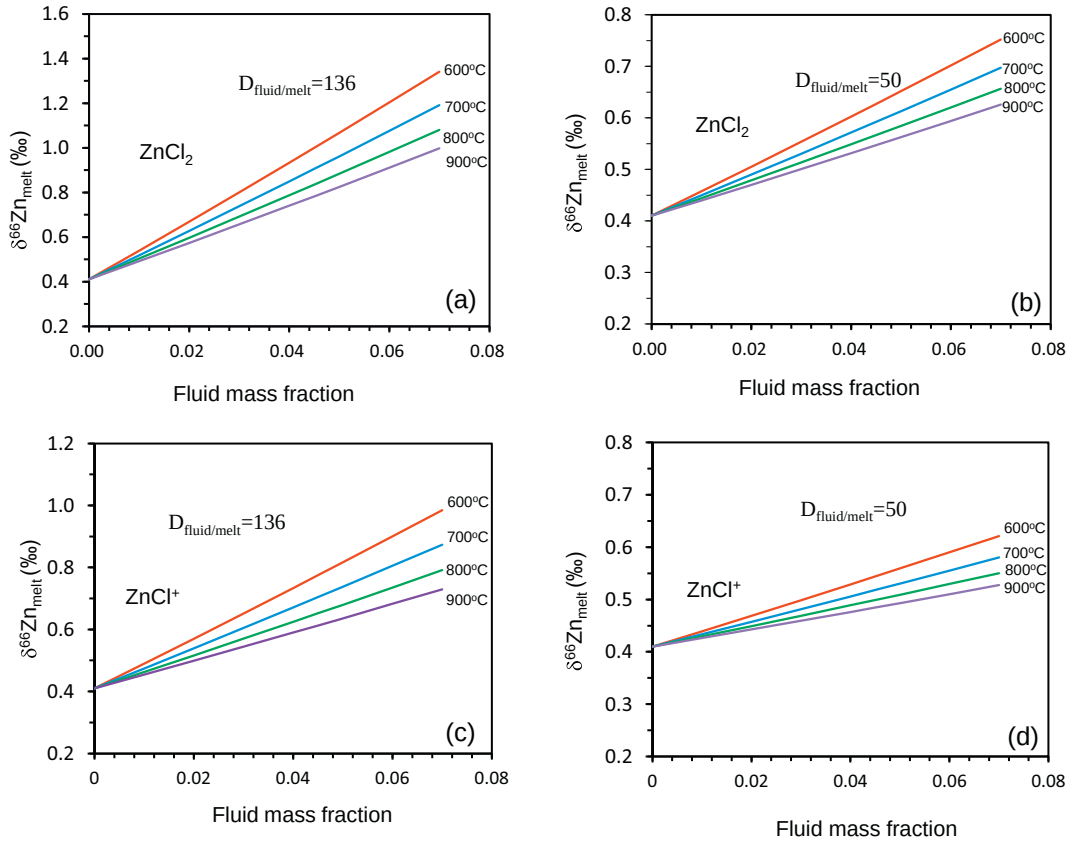

Fig. 8. (a, b) Rayleigh fractionation models for $\delta^{66}Zn$ of the remaining melt and fraction of fluid released from the melt during fluid exsolution. The four curves were calculated by combining the fluid–melt Zn fractionation factors for $ZnCl_2$ and $ZnCl^+$ at 600 °C, 700 °C, 800 °C, and 900 °C, and using the same Zn fluid–melt partition coefficient in each case ($D^{vapor/melt}$).

(up to 0.76‰) with high $(Th/U)_{L/M}$ ratios (8–29). The different $\delta^{66}Zn$ values for the Group I leucosomes may be related to the different temperatures and types of exsolved fluids.

Based on the absence of anhydrous minerals (e.g., orthopyroxene) and the presence of carbonates, $H_2O + CO_2$ fluids are suggested to have triggered partial melting of the protoliths of Dabie migmatites at the early stage (Wang et al., 2013). In fluids, $ZnCO_3$ or $ZnHCO_3^+$ typically have higher $\delta^{66}Zn$ values than free Zn^{2+}, based on results of ab initio calculations (Fujii et al., 2011). Consequently, the influx of $H_2O + CO_2$ fluids should produce elevated $\Delta^{66}Zn_{L-M}$. However, most of the studied leucosomes have similar LOI values at different $\Delta^{66}Zn_{L-M}$ values (Fig. 7b). In addition, one melanosome (0907MSH-1-A) with high CaO content (24.93 wt%) and LOI value (9.94 wt%) has a $\delta^{66}Zn$ value (0.25‰ ± 0.05‰) comparable to those with low CaO and LOI values (Table A1). These observations indicate that the influx of $H_2O + CO_2$ fluids had a limited effect on Zn isotopic compositions during partial melting of the protoliths for migmatites.

5.2. Fractional crystallization

Plagioclase accumulation was documented in the Group III trondhjemitic leucosomes. Group III leucosomes have cumulate textures comprising equant subhedral to euhedral plagioclase and quartz crystals. This texture, and positive Sr–Eu* anomalies and low REE contents (Fig. 4c), indicate that Group III leucosomes have experienced plagioclase accumulation (Wang et al., 2013). Zn^{2+} (0.74 Å) has a similar ionic radius to Mg^{2+} (0.72 Å) and Fe^{2+} (0.78 Å) (Shannon, 1976), and thus it can substitute Mg^{2+} or Fe^{2+} in plagioclase. After excluding samples that were affected by fluid exsolution, the $\Delta^{66}Zn_{L-M}$ values of three remaining Group III samples (0907-MSH-5-B, 0907-MSH-5-B1,and 0907-GFA-2-B) display a positive correlation with $Zn_{M/L}$ ($Zn_{melanosome}/Zn_{leucosome}$: denotes Zn contents difference between leucosome and complementary melansome) and $Eu^*_{L/M}$ ($Eu_{leucosome}/Eu_{melanosome}$: denotes Eu* difference between leucosome and complementary melansome) (Fig. 8), suggesting the Zn isotopic compositions of leucosomes in these samples were modified by plagioclase accumulation. These samples also have extremely low FeO + MgO (≤0.31 wt%) and Zn (≤7.3 ppm) contents (Fig. 9b and d). Thus, even though Zn has a much lower partition coefficient in plagioclase (as low as 0.035; Ewart and Griffin, 1994) than in ferromagnesian minerals (e.g., $D_{amphibole-melt} > 2$, $D_{biotite-melt} > 11$, and $D_{Fe-Ti\ oxide-melt} > 12$; Ewart and Griffin, 1994), when plagioclase is very abundant and becomes the major Zn-bearing phase in a rock (up to 50 vol%), plagioclase accumulation will have a significant influence on the $\delta^{66}Zn$ values, and thus on the $\Delta^{66}Zn_{L-M}$ values of the leucosome–melanosome pairs. The trondhjemitic leucosomes contain mainly plagioclase (35%–50%), quartz (45%–60%), K-feldspar (1%–5%), and biotite (<1%) (Wang et al., 2013). The Zn concentrations of plagioclase (0907-MSH-5B; leucosome), K-feldspar (0907-MSH-5B; leucosome) and biotite (0907-MSH-5A; melanosome) are 2.55, 1.02, and 198.69 ppm, respectively, similar to Zn contents in plagioclase (0.86–3.26 ppm) from high-silica peraluminous granite (Bea et al., 1994), and in biotite (49–368 ppm) from high-silica rocks (Ewart and Griffin, 1994). The sample that shows plagioclase accumulation (0907-MSH-5B1) contains 3.21 ppm Zn, and plagioclase is the dominant host for Zn in this sample. Thus, the $\delta^{66}Zn$ value of plagioclase should be close to that of the host rock 0907-MSH-5B1 (0.49% ± 0.05‰). Modeling of binary mixing between biotite and plagioclase was used to calculate the influence of plagioclase accumulation for the three migmatites (0907-MSH-5-(A, B), 0907-MSH-5-(A1, B1), and 0907-GFA-2-(A, B)). $\delta^{66}Zn$ values of 0.55‰ and 0.15‰ for plagioclase and biotite, respectively, were used to calculate $\delta^{66}Zn$ vaues of the leucosomes. Fig. 9d and Table 2, show that

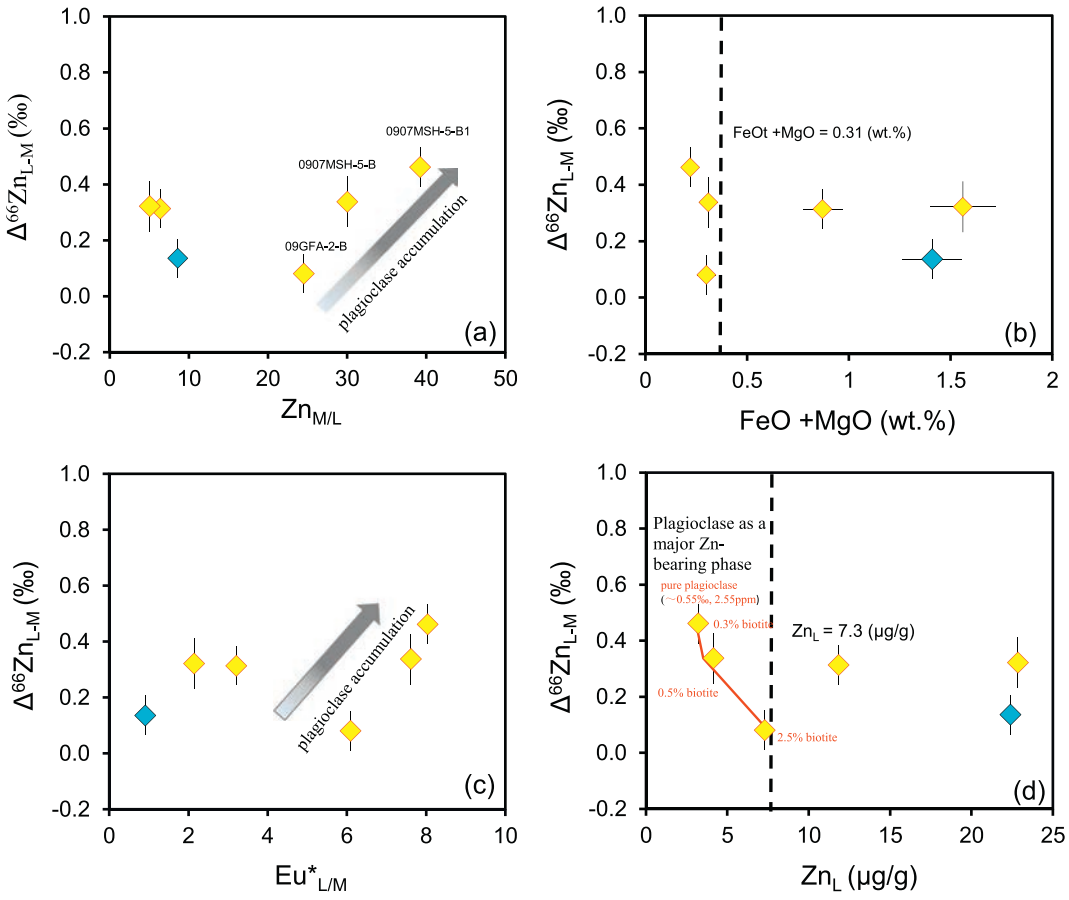

Fig. 9. Plots of $\Delta^{66}Zn_{L-M}$ versus (a) $Zn_{M/L}$, (b) $(FeO + MgO)_L$, (c) $Eu^*_{L/M}$, and (d) Zn_L for leucosomes and melanosomes from the Dabie migmatites. The grey arrows in (a) and (c) show the plagioclase accumulation directions for the leucosomes with low Zn (<7.3 ppm) and FeO + MgO contents (<0.31 wt.%). The red line is the modeled $\Delta^{66}Zn_{L-M}$ values using different biotite and plagioclase compositions, and mass-balance calculations. Biotite contents of 0.3%, 0.5%, and 2.5% are required to produce the $\Delta^{66}Zn_{L-M}$ values of the three samples that have accumulated plagioclase, assuming that all Zn is hosted in plagioclase and biotite. (For interpretation of the references to colour in this figure legend, the reader is referred to the web version of this article.)

when biotite contents in the whole-rocks of the plagioclase accumulative samples are <2.5% (09-GFA-2(A, B); $\Delta^{66}Zn_{L-M}$ = 0.08 ± 0.07‰), plagioclase accumulation would cause Zn isotopic variability in the migmatite. Biotite contents of about 0.3% and 0.5% are needed to generate the isotope offset of other two leucosome and their associated melanosome (0907-MSH-5-(A, B) and 0907-MSH-5-(A1, B1)). Thus, these mass-balance calculations show that plagioclase accumulation might generate high $\delta^{66}Zn$ values in some high-silica granitic rocks (Fig. 9d; Table 2), when plagioclase is the dominant host of Zn in the rock. In this case, these samples are not the right samples to discuss Zn isotope fractionation during partial melting.

The influence of fractional crystallization of other Zn-bearing minerals (Fe–oxides, biotite, and amphibole) on the Zn isotopic systematics of Dabie migmatites was evaluated by plotting $\Delta^{66}Zn_{L-M}$ versus $(FeO + MgO)_{L/M}$ (Fig. 9b). Amphibole, biotite, and Fe–oxides in the melanosome (0907MSH-5-A) are isotopically lighter than in the associated leucosome (Fig. 5). Thus, fractional crystallization of these phases tends to increase the $\delta^{66}Zn$ of the residual melt. Chen et al. (2013) suggest that Zn isotopic fractionation during extreme fractionation of olivine and/or Fe—Ti oxides is <0.1‰. Zinc isotopic variation in the studied leucosomes is much larger than 0.1‰, which is difficult to be explained by fractional crystallization alone, although the crystallization temperature of olivine and Fe—Ti oxides (1100–1200 °C) is higher than the partial melting temperature of the Dabie migmatites (700–820 °C) (Chen et al., 2013;Wang, 1991; Wang et al., 1997; Wang et al., 2013). Of note, the two samples unaffected by fluid exsolution and plagioclase accumulation have similar $\Delta^{66}Zn_{L-M}$ values despite their variable $(FeO + MgO)_{L/M}$ values (Fig. 9b). This further indicates a limited influence of the fractional crystallization of Zn-rich minerals on the Zn isotopic systematics of the studied migmatites.

5.3. Zinc isotope fractionation during crustal melting

Excluding the aforementioned seven samples, two metatexites have identical $\Delta^{66}Zn_{L-M}$ values (0.31‰ and 0.32‰), and another diatexite has a low $\Delta^{66}Zn_{L-M}$ value (0907BJ-2(A, B); 0.14‰ ± 0.07‰) (Fig. 9a). Previous studies have suggested that basaltic melts have Zn isotopic compositions ~0.1‰ heavier than their peridotite source (Wang et al., 2017; Sossi et al., 2018; Huang et al., 2018a, 2018b). Compared with mantle melting, the Dabie migmatites were formed at relatively low temperatures (704–820 °C) (Wang, 1991; Wang et al., 1997; Wang et al., 2013). Doucet et al. (2018) also suggested that ~0.15‰ of disequilibrium kinetic Zn isotopic fractionation can be generated by partial melting of tonalite–trondhjemite–granodiorite rocks, as a result of disequilibrium between the granitic melt and the residue during the rapid formation of granitic magma. If the $\Delta^{66}Zn_{L-M}$ values obtained from the three "unmodified" samples reflect a Zn isotopic fractionation of 0.14‰–0.32‰ due to partial melting of the protoliths, it needs to be considered as to whether the partial melting process was an equilibrium or disequilibrium process.

Theoretical studies suggest that the bonding environment of elements determines the magnitude of equilibrium isotope fractionation, with stronger bonds favoring heavier isotopes (Bigeleisen and Mayer,

1947; Urey, 1947). Minerals with high Zn coordination numbers are expected to preferentially incorporate the light isotopes. General chemical formulae for biotite and amphibole are $[K(Mg,Fe^{2+})_3(Al,Fe^{3+})Si_3O_{10}(OH,F)_2]$ and $(Na,K)_{0\text{-}1}Ca_2[(Mg,Fe^{2+})_4Al](Si,Al)_8O_{22}(OH)_2]$, respectively, in which Zn^{2+} is bonded to six oxygen atoms and in octahedral coordination (Hawthorne and Oberti, 2007; Le Roux et al., 2010; Shannon, 1976). Thus, the higher coordination of oxygen in Zn—O bonds in biotite and amphibole would result in weaker Zn—O bonding strength. Consequently, biotite and amphibole should be depleted in heavy Zn isotopes relative to minerals with tetrahedral coordination. Zinc in magnetite tends to exist in four-fold coordination, with a normal spinel crystal structure (O'Neill and Dollase, 1994). Thus, Zn^{2+} in magnetite is expected to have higher $\delta^{66}Zn$ than silicate minerals (biotite and amphibole). The obtained $\delta^{66}Zn$ value for Fe–oxides (0.21‰) is indeed higher than those of biotite (0.15‰), amphibole (0.16‰), and whole rock (0.15‰). Zinc is usually in tetrahedral coordination in high-silica melts with low NBO/T (Kohn and Schofield, 1994). Thus, assuming equilibrium between all mineral phases and melt, the leucosomes should be enriched in heavy Zn isotopes compared to the melanosomes.

Dauphas et al. (2014) proposed that the force constant of Fe^{2+}–O bond in granite with $SiO_2 > 70$ wt% are stronger than that in less silicic rocks, based on studies of nuclear resonant inelastic X-ray scattering (NRIXS). Given that Zn^{2+} mainly replaces Fe^{2+} and Mg^{2+} in the minerals of granites, difference in force constants of Zn—O bonding between melt and residual are expected to be the major mechanism controlling Zn isotope fractionation during the generation of granitic melts. It is important to evaluate whether the observed Zn isotope fractionation is an equilibrium process or the result of kinetic isotopic effects. Sossi et al. (2018) proposed that the equilibrium Zn isotopic fractionation factor between basalt (melt) and residue is $\Delta^{66}Zn_{melt-residual} = +0.17 \times 10^6/T^2$ (T in K), which is due to the different coordination numbers of $^{VI}Zn^{2+}$ (residue) and $^{IV}Zn^{2+}$ (melt). This formula can be extended to a granitic magmatic system. The partial melting temperature of the Dabie migmatites was 700–800 °C (Wang et al., 2013). The calculated equilibrium Zn isotope fractionation factor between leucosomes and melansomes ($\Delta^{66}Zn_{leucosome-melanosome}$) for the studied metatexites is +0.14‰ to +0.18‰, based on the above formula. The $\Delta^{66}Zn_{L-M}$ values (0.31‰–0.32‰) of the Dabie metatexitic migmatites are higher than these calculated values, and possibly reflect kinetic isotopic effects due to rapid melt segregation during partial melting of the migmatite protoliths. In contrast, the $\Delta^{66}Zn_{L-M}$ value (0907BJ-2(A, B); 0.14‰ ± 0.08‰) for the diatexite is consistent with the calculated equilibrium fractionation value, possibly indicating equilibrium Zn isotopic fractionation. Two orthogneisses from the Dabie orogenic belt, which represent the protoliths of the Dabie migmatites (Wang et al., 2013), have $\delta^{66}Zn$ values (0.24‰ ± 0.05‰ and 0.27‰ ± 0.05‰; Table 1) similar to those of global oceanic basalts (0.28‰ ± 0.03‰; Wang et al., 2017). We assume that the $\delta^{66}Zn$ value of the diatexitic leucosome (0907BJ-2-B) source is similar to those of the two orthogneisses, which indicates that ~0.16‰ of Zn isotopic fractionation ($\Delta^{66}Zn_{leucosome-orthogneiss}$) occurred during melting of the orthogneiss. This value is consistent with those calculated for the Dabie migmatites.

5.4. Implications for Zn isotopic variations in high-silica granites

Granitoids represent one of the most important components of the continental crust, and record melting processes in the continental crust (e.g., Foden et al., 2015; Turner et al., 1992). Previous studies have suggested that silicic rocks ($SiO_2 > 70$ wt%; MgO < 0.6 wt%) have heavier Fe isotopic compositions than mafic to intermediate igneous rocks in the crust. Fluid exsolution, fractional crystallization, partial melting, source heterogeneity, diffusion, and/or coordination number have been invoked to explain the stable isotopic compositions of silicic rocks (e.g., Foden et al., 2015; Heimann et al., 2008; Poitrasson and Freydier, 2005; Schuessler et al., 2009; Sossi et al., 2012; Telus et al., 2012; Teng et al., 2011; Zambardi et al., 2014). Zinc is different from Fe, and only has one valence (Zn^{2+}). Nevertheless, significant Zn isotopic variations in felsic/granitic rocks (0.12‰–0.88‰) have also been observed in the crust (Telus et al., 2012; Doucet et al., 2018; Xia et al., 2017; Huang et al., 2018b; this study) (Fig. 1). Four granites from the Dabie orogenic belt have $\delta^{66}Zn$ values from 0.28‰ ± 0.05‰ to 0.41‰ ± 0.05‰ and SiO_2 contents from 69.3 to 77.5 wt%. There is a general increase of $\delta^{66}Zn$ with increasing SiO_2 (Fig. 1). Thus, our data also show that high-silica granites ($SiO_2 > 70$ wt%) have higher $\delta^{66}Zn$ values than more mafic rocks ($SiO_2 < 70$ wt%) (Fig. 1). Together with the granite data from Doucet et al. (2018), it is also clear that the Zn isotopic ratios of high-silica granites ($SiO_2 > 70$ wt%) are generally higher than those of global oceanic basalts (0.28‰ ± 0.05‰; Chen et al., 2013; Wang et al., 2017; Huang et al., 2018b) (Fig. 1). The Mg, Si and Ti isotopes also show similar behavior (Greber et al., 2017; Savage et al., 2011, 2012; Telus et al., 2012; Teng et al., 2010; Zambardi et al., 2014; Zhu et al., 2015). Thus, the Zn isotope can be used to trace the processes of crust differentiation.

The migmatite data obtained in this study suggest that crustal melting can produce +0.14‰ to +0.18‰ Zn isotope fractionation between silicic melts and residues. However, this fractionation is much smaller than the overall variation observed in high-silica granites. Thus, additional processes such as fluid exsolution and plagioclase accumulation, all of which have been demonstrated to significantly fractionate Zn isotopes in this study, must also contribute to the Zn isotopic heterogeneity of high-silica igneous rocks. It is notable that some high-silica granitic rocks ($SiO_2 > 70$ wt%) have Zn isotopic compositions comparable to those of global oceanic basalts (Fig. 1), which may have been caused by the Zn isotopic heterogeneity of the granite protolith.

6. Conclusions

Leucosomes, melanosomes, and amphibolitic schollens in the Dabie migmatites were analyzed for Zn isotopes to investigate Zn isotope fractionation during differentiation of the continental crust. All of the studied leucosomes have higher $\delta^{66}Zn$ values than associated melanosomes, with $\Delta^{66}Zn_{L-M}$ ranging from 0.08‰ ± 0.07‰ to 0.76‰ ± 0.07‰. The high $(Th/U)_{L/M}$ ratios of four metatexitic leucosomes suggest that fluid exsolution is the main cause of the large $\Delta^{66}Zn_{L-M}$ variations (up to 0.76‰ ± 0.07‰). $\Delta^{66}Zn_{L-M}$ values for three samples (0.08‰ ± 0.07‰ to 0.46‰ ± 0.07‰; 0907-MSH-5-B; 0907-MSH-5-B1 and 09-GFA-2-B) were controlled by plagioclase accumulation, as supported by high plagioclase contents, positive Eu* anomalies, low Zn contents, and mass-balance calculations. The $\Delta^{66}Zn_{L-M}$ value (0.14‰ ± 0.07‰) for the diatexite may reflect equilibrium Zn isotopic fractionation during partial melting.

High-silica granitic rocks ($SiO_2 > 70$ wt%) with higher $\delta^{66}Zn$ values relative to those of more mafic rocks were documented in this study. Our results suggest that Zn isotope equilibrium fractionation of +0.14‰ to +0.18‰ can be generated during crustal anatexis, based on the equilibrium Zn isotope fractionation between basalt and its source residue. However, fluid exsolution and plagioclase accumulation also contribute to the heavy Zn isotopic compositions of high-silica granitic rocks.

Acknowledgement

We appreciated the Dr. Paolo Sossi, Dr. Jian Huang and one anonymous reviewer for their constructive comments and efficient editorial handling of chief editor Xianhua Li. We thank S.-J. Wang,Y.S. He and Q. X. Xia for supplying the samples, and H. Sun, Y.S. He and R.H. Gao for comments and language editing on this version of the manuscript. This work was supported by the National Natural Science Foundation of China (Grant Nos. 41403010, and 41622303), the Fundamental Research Funds for the Central Universities (Grant No. 292014064 to

LJX), and the "Strategic Priority Research Program" of the Chinese Academy of Sciences (Grant No. XDB18030603 to SAL).

Appendix A. Supplementary data

Supplementary data to this article can be found online at https://doi.org/10.1016/j.lithos.2018.11.028.

References

Ashworth, J.R. (Ed.), 1985. Migmatites. Blackie, Glasgow and London.

Bea, F., Pereira, M.D., Stroh, A., 1994. Mineral/leucosome trace-element partitioning in a peraluminous migmatite (a laser ablation-ICP-MS study). Chemical Geology 117 (1–4), 291–312.

Bigeleisen, J., Mayer, M.G., 1947. Calculation of equilibrium constants for isotopic exchange reactions. The Journal of Physical Chemistry 13, 261–267.

Brown, M., 2001. Orogeny, migmatites and leucogranites: a review. Journal of Earth System Science 110 (4), 313–336.

Brown, M., 2007. Crustal melting and melt extraction, ascent and emplacement in orogens: mechanisms and consequences. Journal of the Geological Society 164, 709–730.

Carswell, D.A., Wilson, R.N., Zhai, M.G., 2000. Metamorphic evolution, mineral chemistry and thermobarometry of schists and orthogneisses hosting ultra-high pressure eclogites in the Dabieshan of Central China. Lithos 52, 121–155.

Chen, H., Savage, P.S., Teng, F.-Z., Helz, R.T., Moynier, F., 2013. Zinc isotope fractionation during magmatic differentiation and the isotopic composition of the bulk Earth. Earth and Planetary Science Letters 369–370 (0), 34–42.

Cong, B.L., 1996. Ultrahigh-pressure Metamorphic Rocks in the Dabieshan-Sulu Region of China. Science Press, Beijing, pp. 1–224.

Dauphas, N., Roskosz, M., Alp, E..E., Neuville, D.R., Hu, M.Y., Sio, C.K., Tissot, F.L.H., Zhao, J., Tissandier, L., Médard, E., Cordier, C., 2014. Magma redox and structural controls on iron isotope variations in Earth's mantle and crust. Earth and Planetary Science Letters 398, 127–140.

Doucet, L.S., Laurent, O., Mattielli, N., Debouge, W., 2018. Zn isotope heterogeneity in the continental lithosphere: New evidence from Archean granitoids of the northern Kaapvaal craton, South Africa. Chemical Geology 476, 260–271.

Du, D.H., Wang, X.L., Yang, T., Chen, X., Li, J.Y., Li, W., 2017. Origin of heavy Fe isotope compositions in high-silica igneous rocks: a rhyolite perspective. Geochimica et Cosmochimica Acta 218, 58–72.

Ducher, M., Blanchard, M., Balan, E., 2016. Equilibrium zinc isotope fractionation in Zn bearing minerals from first-principles calculations. Chemical Geology 443, 87–96.

Ducher, M., Blanchard, M., Balan, E., 2018. Equilibrium isotopic fractionation between aqueous Zn and minerals from first-principles calculations. Chemical Geology 483, 342–350.

Ewart, L., Griffin, W.L., 1994. Application of proton microprobe data to trace-element partitioning in volcanic rocks. Chemical Geology 117, 251–284.

Foden, J., Sossi, P.A., Wawryk, C.M., 2015. Fe isotopes and the contrasting petrogenesis of A-, I- and S-type granite. Lithos 212-215, 32–44.

Fujii, T., Moynier, F., Pons, M.L., Albarède, F., 2011. The origin of Zn isotope fractionation in sulfides. Geochimica et Cosmochimica Acta 75 (23), 7632–7643.

Greber, N.D., Dauphas, N., Bekker, A., Ptáček, M.P., Bindeman, I.N., Hofmann, A., 2017. Titanium isotopic evidence for felsic crust and plate tectonics 3.5 billion years ago. Science 357 (6357), 1271–1274.

Hawkesworth, C.J., Turner, S.P., McDermott, F., Peate, D.W., van Calsteren, P., 1997. U-Th isotopes in arc magmas: Implications for element transfer from the subducted crust. Science 276 (5312), 551–555.

Hawthorne, F.C., Oberti, R., 2007. Amphiboles: crystal chemistry. Reviews in Mineralogy and Geochemistry 67, 1–54.

He, Y., Li, S., Hoefs, J., Huang, F., Liu, S.A., Hou, Z., 2011. Post-collisional granitoids from the Dabie orogen: new evidence for partial melting of a thickened continental crust. Geochimica et Cosmochimica Acta 75 (13), 3815–3838.

He, Y., Li, S., Hoefs, J., Kleinhanns, I.C., 2013. Sr-Nd-Pb isotopic compositions of early cretaceous granitoids from the Dabie orogen: constraints on the recycled lower continental crust. Lithos 156, 204–217.

He, Y., Wu, H., Ke, S., Liu, S.A., Wang, Q., 2017. Iron isotopic compositions of adakitic and non-adakitic granitic magmas: Magma compositional control and subtle residual garnet effect. Geochimica et Cosmochimica Acta 203, 89–102.

Heimann, A., Beard, B.L., Johnson, C.M., 2008. The role of volatile exsolution and subsolidus fluid/rock interactions in producing high $^{56}Fe/^{54}Fe$ ratios in siliceous igneous rocks. Geochimica et Cosmochimica Acta 72, 4379–4396.

Huang, F., Li, S.G., Dong, F., He, Y.S., Chen, F.K., 2008. High-Mg adakitic rocks in the Dabie orogen, Central China: implications for foundering mechanism of lower continental crust. Chemical Geology 255 (1–2), 1–13.

Huang, J., Liu, S.-A., Wo¨rner, G., Yu, H., Xiao, Y., 2016. Copper isotope behavior during extreme magma differentiation and degassing: a case study on Laacher See phonolite tephra (East Eifel, Germany). Contributions to Mineralogy and Petrology 171, 1–16.

Huang, J., Chen, S., Zhang, X.C., Huang, F., 2018a. Effects of melt percolation on Zn isotope heterogeneity in the mantle: constraints from peridotite Massifs in Ivrea-Verbano Zone, Italian Alps. Journal of Geophysical Research: Solid Earth 123 (4), 2706–2722.

Huang, J., Zhang, X.C., Chen, S., Tang, L.M., Worner, G., Yu, H.M., Huang, F., 2018b. Zinc isotopic systematics of Kamchatka-Aleutian arc magmas controlled by mantle melting. Geochimica et Cosmochimica Acta 238, 85–101.

Kohn, S.C., Schofield, P.F., 1994. The importance of melt composition in controlling trace-element behaviour: an experimental study of Mn and Zn partitioning between forsterite and silicate melts. Chemical Geology 117 (1–4), 73–87.

Laurent, O., Martin, H., Moyen, J.F., Doucelance, R., 2014. The diversity and evolution of late-Archean granitoids: evidence for the onset of "modern-style" plate tectonics between 3.0 and 2.5Ga. Lithos 205, 208–235.

Le Roux, V., Lee, C.T., Turner, S.J., 2010. Zn/Fe systematics in mafic and ultramafic systems: implications for detecting major element heterogeneities in the Earth's mantle. Geochimica et Cosmochimica Acta 74 (9), 2779–2796.

Li, S.G., et al., 1993. Collision of the North China and Yangtze Blocks and formation of coesite-bearing eclogites: timing and processes. Chemical Geology 109, 89–111.

Li, S.G., Jagoutz, E., Chen, Y., Li, Q., 2000. Sm-Nd and Rb-Sr isotopic chronology and cooling history of ultrahigh pressure metamorphic rocks and their country rocks at Shuanghe in the Dabie Mountains, Central China. Geochimica et Cosmochimica Acta 64, 1077–1093.

Li, S.G., Huang, F., Nie, Y.H., Han, W.L., Long, G., Li, H.M., Zhang, S.Q., Zhang, Z.H., 2001. Geochemical and geochronological constraints on the suture location between the North and South China blocks in the Dabie Orogen, Central China. Physics and Chemistry of the Earth, Part A: Solid Earth and Geodesy A26, 655–672.

Li, S.G., Li, Q., Hou, Z., Yang, W., Wang, Y., 2005. Colling history and exhumation mechanism of the ultrahigh-pressure metarmophic rocks in the Dabie Moutains, central China. Acta Petrologica Sinica 21, 11 17–1124.

Liu, J.B., Ye, K., Maruyama, S., Cong, B.L., Fan, H.R., 2001. Mineral inclusions in zircon from gneisses in the ultrahigh-pressure zone of the Dabie Mountains, China. Journal of Geology 109, 523–535.

Liu, S.-A., Teng, F.Z., He, Y., Ke, S., Li, S., 2010a. Investigation of magnesium isotope fractionation during granite differentiation: implication for Mg isotopic composition of the continental crust. Earth and Planetary Science Letters 297 (3), 646–654.

Liu, Y.C., Gu, X.F., Li, S.G., Hou, Z.H., Song, B., 2010b. Multistage metamorphic events in granulitized eclogites from the NortDabie complex zone, central China: evidence from zircon U–Pb age, trace element and mineral inclusion. Lithos 122, 107–121.

Liu, S.-A., Li, D., Li, S., Teng, F., Ke, S., He, Y., Lu, Y., 2014. High-precision copper and iron isotope analysis of igneous rock standards by MC-ICP-MS. Journal of Analytical Atomic Spectrometry 29 (1), 122–133.

Liu, S.-A., Wang, Z.Z., Li, S., Huang, J., Yang, W., 2016. Zinc isotope evidence for a large-scale carbonated mantle beneath eastern China. Earth and Planetary Science Letters 444, 169–178.

Liu, S.-A., Wu, H., Shen, S.Z., Jiang, G., Zhang, S., Lv, Y., Zhang, H., Li, S.G., 2017. Zinc isotope evidence for intensive magmatism immediately before the end-Permian mass extinction. Geology 45 (4), 343–346.

Lv, Y., Liu, S.A., Zhu, J.M., Li, S., 2016. Copper and zinc isotope fractionation during deposition and weathering of highly metalliferous black shales in central China. Chemical Geology 445, 24–35.

Mason, T.F., Weiss, D.J., Horstwood, M., Parrish, R.R., Russell, S.S., Mullane, E., Coles, B.J., 2004. High-precision Cu and Zn isotope analysis by plasma source mass spectrometry part 1. Spectral interferences and their correction. Journal of Analytical Atomic Spectrometry 19 (2), 209–217.

McDonough, W.F., Sun, S.S., 1995. The Composition of the Earth. Chemical Geology 120, 223–254.

O'Neill, H.S.C., Dollase, W.A., 1994. Crystal structures and cation distributions in simple spinels from powder XRD structural refinements: $MgCr_2O_4$, $ZnCr_2O_4$, Fe_3O_4 and the temperature dependence of the cation distribution in $ZnAl_2O_4$. Physics and Chemistry of Minerals 20 (8), 541–555.

Poitrasson, F., Freydier, R., 2005. Heavy iron isotope composition of granites determined by high resolution MC-ICP-MS. Chemical Geology 222, 132–147.

Rudnick, R.L., Gao, S., 2003. Composition of the continental crust. Treatise on geochemistry 3, 659.

Rubatto, D., Hermann, J., 2007. Experimental zircon/melt and zircon/garnet trace element partitioning and implications for the geochronology of crustal rocks. Chemical Geology 241 (1–2), 38–61.

Savage, P.S., Georg, R.B., Williams, H.M., Burton, K.W., Halliday, A.N., 2011.. Silicon isotope fractionation during magmatic differentiation. Geochimica et Cosmochimica Acta 75, 6124–6139. https://doi.org/10.1016/j.gca.2011.07.043.

Savage, P.S., Georg, R.B., Williams, H.M., Turner, S., Halliday, A.N., Chappell, B.W., 2012. The silicon isotope composition of granites. Geochimica et Cosmochimica Acta 92, 184–202.

Sawyer, E.W., 2008. Working with migmatites: nomenclature for the constituent parts. Work Migmatites Mineral Assoc Can Short Course Ser 38, 1–28.

Sawyer, E.W., Cesare, B., Brown, M., 2011. When the continental crust melts. Elements 7, 229–234.

Schuessler, J.A., Schoenberg, R., Sigmarsson, O., 2009. Iron and lithium isotope systematics of the Hekla volcano, Iceland -evidence for Fe isotope fractionation during magma differentiation. Chemical Geology 258 (1–2), 78–91.

Shannon, R.D., 1976. Revised effective ionic radii and systematic studies of interatomie distances in halides and chaleogenides. Acta Crystallographica Section a: Crystal Physics, Diffraction, Theoretical and General Crystallography 32, 751–767.

Sigurdsson, H., Houghton, B., McNutt, S., Rymer, H., Stix, J. (Eds.), 2015. The Encyclopedia of Volcanoes. Elsevier.

Sossi, P., Foden, J., Halverson, G., 2012. Redox-controlled iron isotope fractionation during magmatic differentiation: an example from the Red Hill intrusion, S. Tasmania. Contributions to Mineralogy and Petrology 164, 757–772. https://doi.org/10.1007/s00410–012–0769–x.

Sossi, P.A., Halverson, G.P., Nebel, O., Eggins, S.M., 2015. Combined separation of Cu, Fe and Zn from rock matrices and improved analytical protocols for stable isotope determination. Geostandards and Geoanalytical Research 39 (2), 129–149.

Sossi, P.A., Nebel, O., O'Neill, H.S.C., Moynier, F., 2018. Zinc isotope composition of the Earth and its behaviour during planetary accretion. Chemical Geology 477, 73–84.

Telus, M., Dauphas, N., Moynier, F., Tissot, F.L.H., Teng, F.-Z., Nabelek, P.I., Craddock, P.R., Groat, L.A., 2012. Iron, zinc, magnesium and uranium isotope fractionation during continental crust differentiation: the tale from migmatites, granitoids, and pegmatites. Geochimica et Cosmochimica Acta 97, 247–265.

Teng, F.Z., Li, W.Y., Ke, S., Marty, B., Dauphas, N., Huang, S., Wu, F., Pourmand, A., 2010. Magnesium isotopic composition of the Earth and chondrites. Geochimica et Cosmochimica Acta 74 (14), 4150–4166.

Teng, F.Z., Dauphas, N., Helz, R.T., Gao, S., Huang, S., 2011. Diffusion-driven magnesium and iron isotope fractionation in Hawaiian olivine. Earth and Planetary Science Letters 308 (3–4), 317–324.

Turner, S.P., Foden, J., Morrison, R.S., 1992. Derivation of some A-type magmas by fractionation of basaltic magma: an example from the Padthaway Ridge, South Australia. Lithos 28, 151–179.

Urey, H.C., 1947. The thermodynamic properties of isotopic substances. Journal of the Chemical Society 562–581 (Resumed).

Wang, J.H., 1991. The Early Evolution of the Dabie Complex, with Special Reference to the Genetic Mechanism of Migmatites. China University of Geosciences Press, Wuhan (134 pp.).

Wang, J.H., Sun, M., Chang, X.Y., Deng, S.X., 1997. Dynamic models for origin of the migmatites with thermal centers in the Dabie complex, Hubei, Central China. In: Qian, X.L., You, Z.D., Jahn, B.M., Halls, H.C. (Eds.), Precambrain Geology and Metamorphic Petrology. Procs. 30th IGC, 17, VSP, Zeist, 203– 215.

Wang, Q., Wyman, D.A., Xu, J.F., Jian, P., Zhao, Z.H., Li, C.F., Xu, W., Ma, J.L., He, B., 2007. Early cretaceous adakitic granites in the Northern Dabie complex, Central China: implications for partial melting and delamination of thickened lower crust. Geochimica et Cosmochimica Acta 71 (10), 2609–2636.

Wang, S.J., Li, S.G., Chen, J., He, Y.S., An, S.C., Shen, J., 2013. Geochronology and geochemistry of leucosomes in the North Dabie Terrane, East China: implication for post-UHPM crustal melting during exhumation. Contributions to Mineralogy and Petrology 165 (5), 1009–1029.

Wang, Z.Z., Liu, S.A., Liu, J., Huang, J., Xiao, Y., Chu, Z.Y., Zhao, X.M., Tang, X.-M., 2017. Zinc isotope fractionation during mantle melting and constraints on the Zn isotope composition of Earth's upper mantle. Geochimica et Cosmochimica Acta 198, 151–167.

Wimmenauer, W., Bryhni, I., 2002. Towards a unified nomenclature of metamorphic petrology: migmatites and related rocks. A Proposal on Behalf of the IUGS Subcommission on the Systematics of Metamorphic Rocks, Web Version of 31 July 2002.

Wu, H., He, Y., Bao, L., Zhu, C., Li, S., 2017. Mineral composition control on inter-mineral iron isotopic fractionation in granitoids. Geochimica et Cosmochimica Acta 198, 208–217.

Xia, Q.X., Wang, H.Z., Zhou, L.G., Gao, X.Y., Zheng, Y.F., Van Orman, J., Xu, H.J., Hu, Z.C., 2016. Growth of metamorphic and peritectic garnets in ultrahigh-pressure metagranite during continental subduction and exhumation in the Dabie orogen. Lithos 266, 158–181.

Xia, Y., Li, S., Huang, F., 2017. Iron and Zinc isotope fractionation during magmatism in the continental crust: evidence from bimodal volcanic rocks from Hailar basin, NE China. Geochimica et Cosmochimica Acta. 213, 35–46.

Xu, S.T., Okay, A.I., Ji, S.Y., Sengor, A.M.C., Su, W., Liu, Y.C., Jiang, L.L., 1992. Diamond from the Dabie Shan metamorphic rocks and its implication for tectonic setting. Science 256, 80–82.

Xu, L., Xiao, Y., Wu, F., Li, S., Simon, K., Wörner, G., 2013. Anatomy of garnets in a Jurassic granite from the south-eastern margin of the North China Craton: magma sources and tectonic implications. Journal of Asian Earth Sciences 78, 198–221.

Xu, L., Y. S. He, S. J. Wang, H. J. Wu, S, J., Wang, and S. G. Li (2017), Iron isotope fractionation during crustal anatexis: Constraints from migmatites from the Dabie orogen, Central China, Lithos, 284–285, 171–179.

Zajacz, Z., Halter, W.E., Pettke, T., Guillong, M., 2008. Determination of fluid/melt partition coefficients by LAICPMS analysis of co-existing fluid and silicate melt inclusions: controls on element partitioning. Geochimica et Cosmochimica Acta 72, 2169–2197.

Zambardi, T., Lundstrom, C.C., Li, X., McCurry, M., 2014. Fe and Si isotope variations at Cedar Butte volcano; insight into magmatic differentiation. Earth and Planetary Science Letters 405, 169–179.

Zheng, Y.-F., Wu, Y.-B., Zhao, Z.-F., Zhang, S.-B., Xu, P., Wu, F.-Y., 2005. Metamorphic effect on zircon Lu-Hf and U–Pb isotope systems in ultrahigh-pressure metagranite and metabasite. Earth and Planetary Science Letters 240, 378–400.

Zhu, D., Bao, H., Liu, Y., 2015. Non-traditional stable isotope behaviors in immiscible silica-melts in a mafic magma chamber. Scientific Reports 5, 17561.